Supplementary information

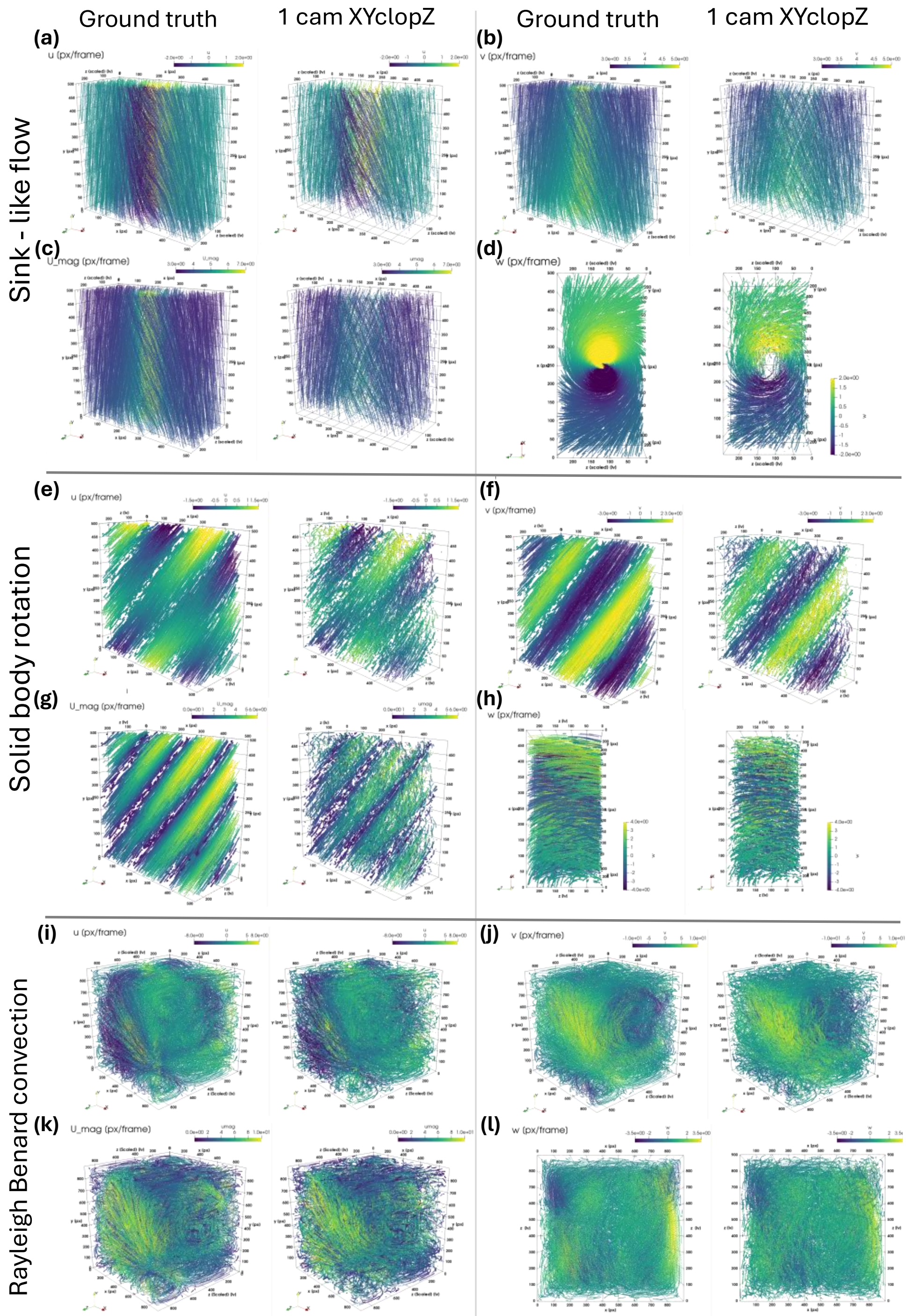

*Supplementary Fig. 1 Comparison for the ground truth tracks vs the single camera XYclopZ-LPT velocity results. Panels **(a-d)** show results for the sink-like flow case, while panels **(e-h)** and **(i-l)** show the velocity results for the solid body rotation case and the Rayleigh-Bénard convection cases respectively. Panels **(a, e, i)** show 3D views that are colored by velocity component u along the x axis. Panels **(b, f, j)** are colored by the velocity component v along the y axis. Panels **(c, g, k)** are colored by the velocity magnitude. Panels **(d, h, l)** present an XZ top view of the results (not seen by the camera) colored by velocity component w. In each panel, the ground truth is presented on the left while the XYclopZ-LPT result is shown on the right.*

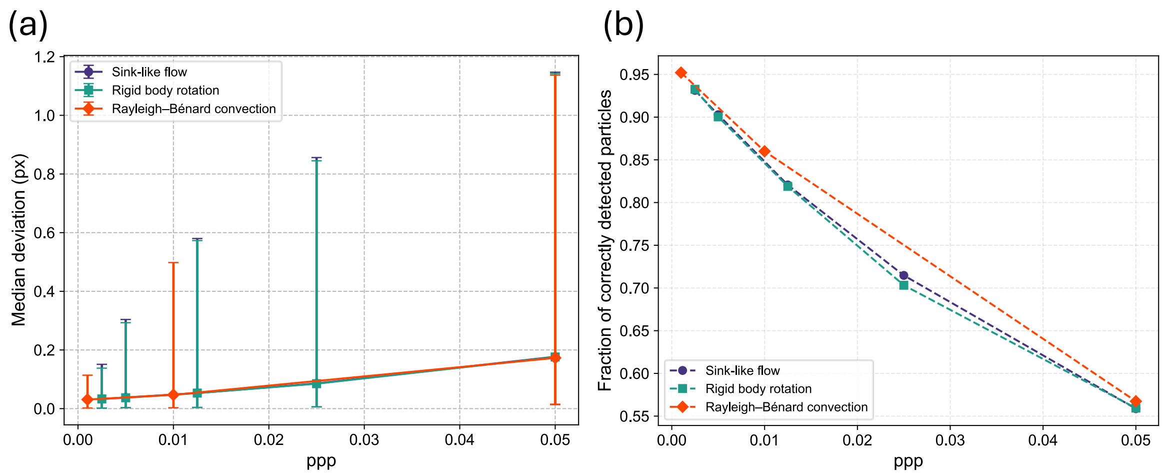

Supplementary Fig. 2 Evaluation of the proposed particle detection method (Section: " 2D Particle detection") using synthetic particle images. ***(a)*** *Euclidean distance deviation (pixels) of detected 2D particle positions from their true locations, plotted against particle seeding density (particles per pixel, ppp). Error bars represent the 5th–95th percentile range of deviations across all particles.* ***(b)*** *Fraction of correctly identified particles relative to the ground truth versus particle concentration for the synthetic datasets analyzed in this study.*

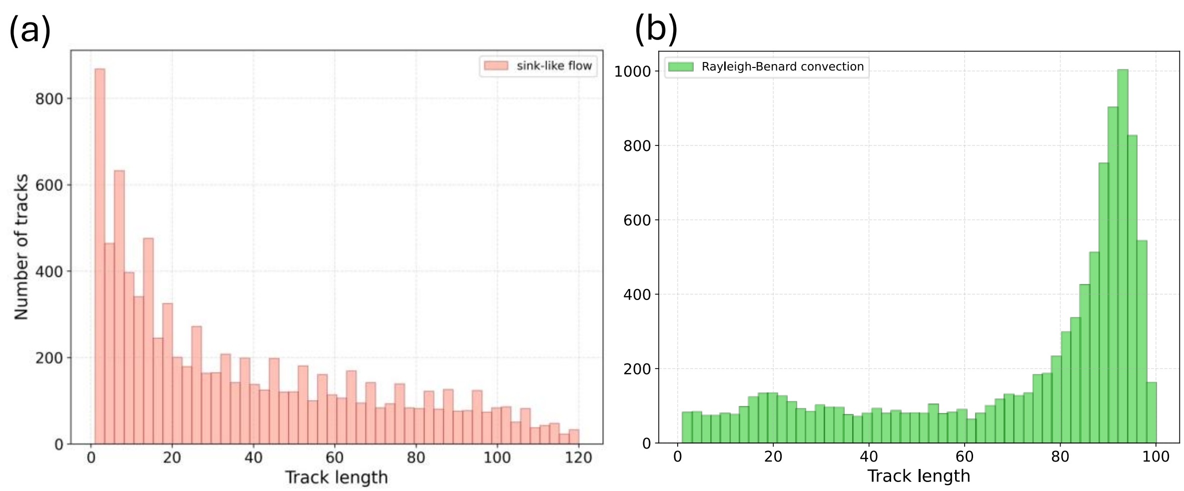

Supplementary Fig. 3 Histograms of track lengths for the ***(a)*** *sink-like flow at 0.0125 ppp and* ***(b)*** *Rayleigh-Bénard convection at 0.01 ppp cases. Note the higher track lengths for the Rayleigh- Bénard convection case due to "trapped" particles in the VOI.*

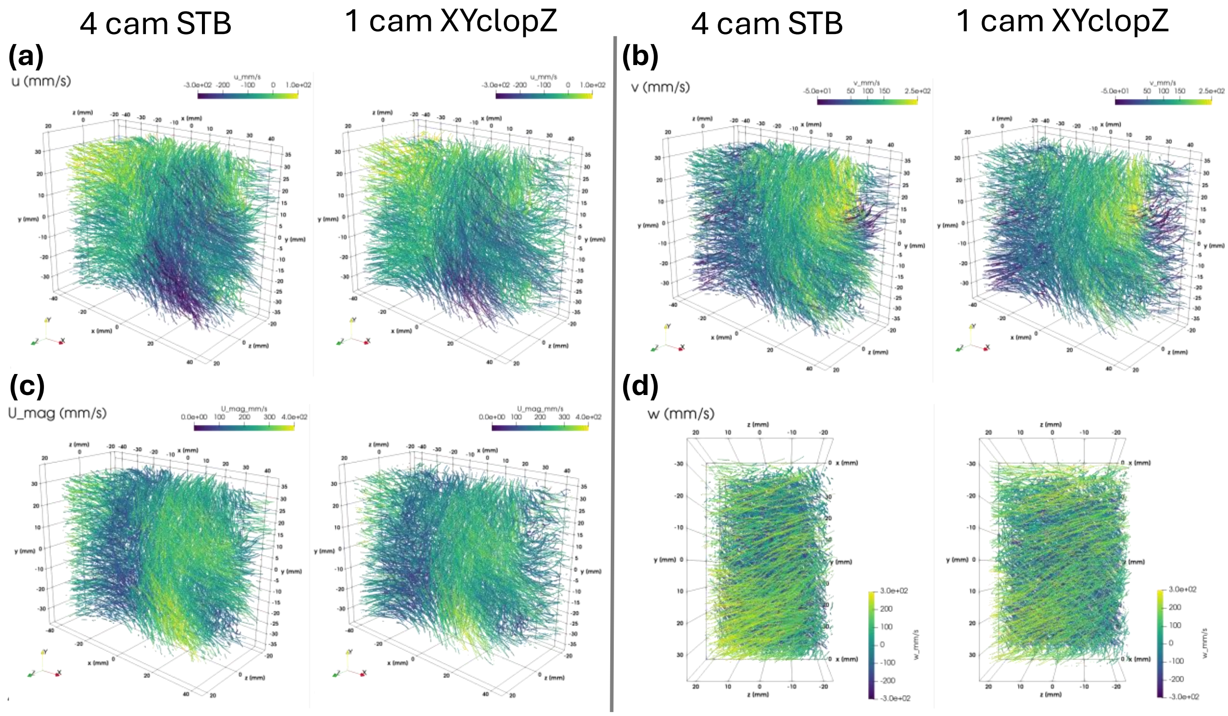

*Supplementary Fig. 4 Benchmark between the STB and single camera XYclopZ-LPT systems. All panels show a side-by-side comparison of the resulting time resolved 3D particle trajectories from the multicamera STB system (left) and single camera XYclopZ-LPT system (right) from a 3D perspective view **(a-c)** and a YZ view **(d)** not directly seen by the camera. All panels show an overlay of 50 consecutive time steps. Panel **(a)** is colored by the u velocity component along the x-axis, **(b)** is colored by the v velocity component along the y-axis, panel **(c)** is colored by the velocity magnitude and panel **(d)** is colored by the w velocity component along z-axis.*

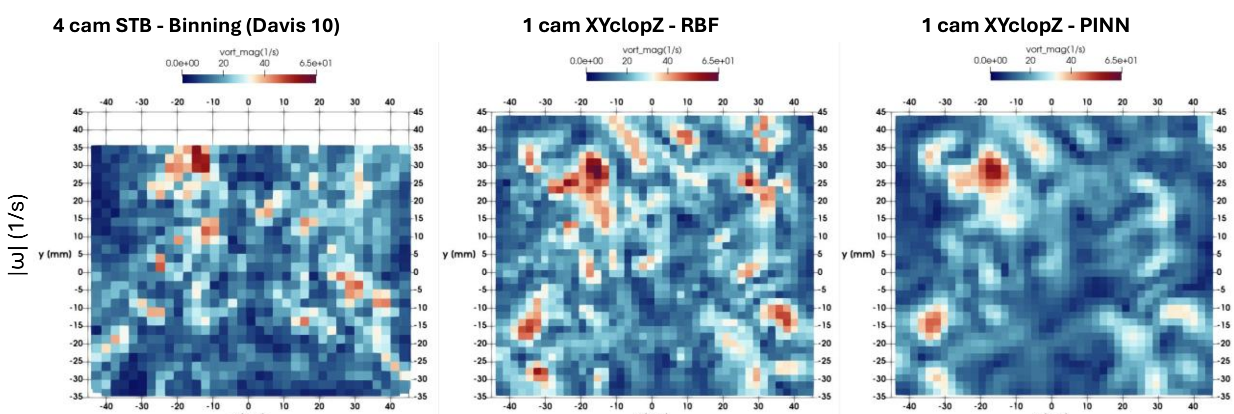

Supplementary Fig. 5 Instantaneous Eulerian vorticity magnitude fields interpolated onto a regular Cartesian grid from the reconstructed 3D particle tracks. Contour plots are shown for the mid-plane (XY slice at z = 0 mm). Panels show the vorticity magnitude ($|\omega|$), derived from their corresponding Eulerian velocity fields for the 4 camera STB system (left), single camera XYclopZ -RBF (center) and single camera XYclopZ – PINN (right). Note that the 4 camera STB system can not resolve the top portion of the volume, due to a reduced overlapped region between the cameras.

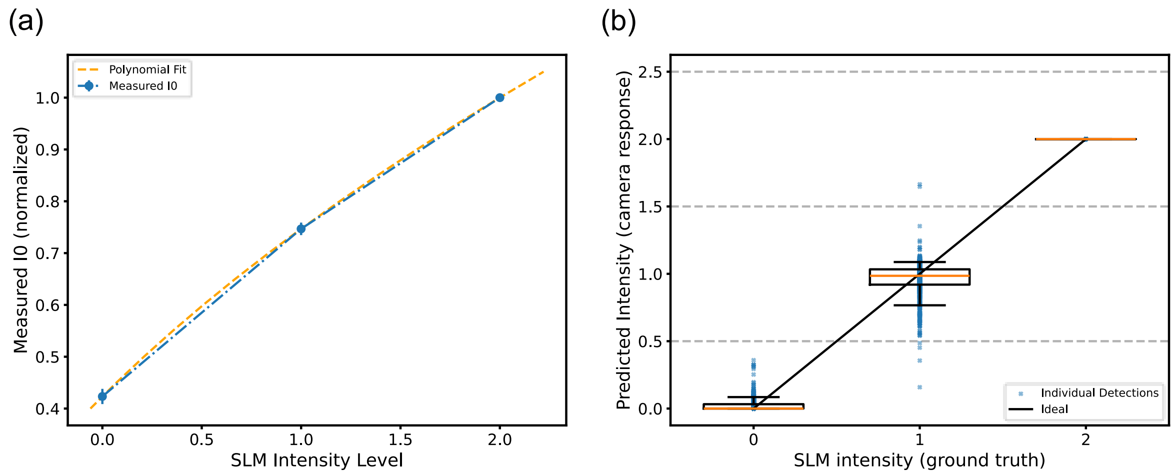

Supplementary Fig. 6 ***(a)*** *Normalized intensity parameter response* $(\overline{I_o})$ *vs SLM true intensity level, error bars show the median absolute deviation of all the data points used to characterize the intensity of the particles.* ***(b)*** *Measured Camera response by mapping* $\overline{I_o}$ *with the polynomial fit vs SLM true intensity. The yellow line represents the median response, the box boundaries represent the* 1^{st} *quartile and* 3^{rd} *quartile of the data, with whiskers representing* 5^{th} *and* 95^{th} *percentile of the data. The gray horizontal dashed lines represent the cutoff values for assigning a detected Intensity. Note that a zero value does not represent black, but rather represents the lowest intensity level (dark gray) index, where an index of 2 is the maximum intensity for a 2-bit structured illumination (maximum intensity).*

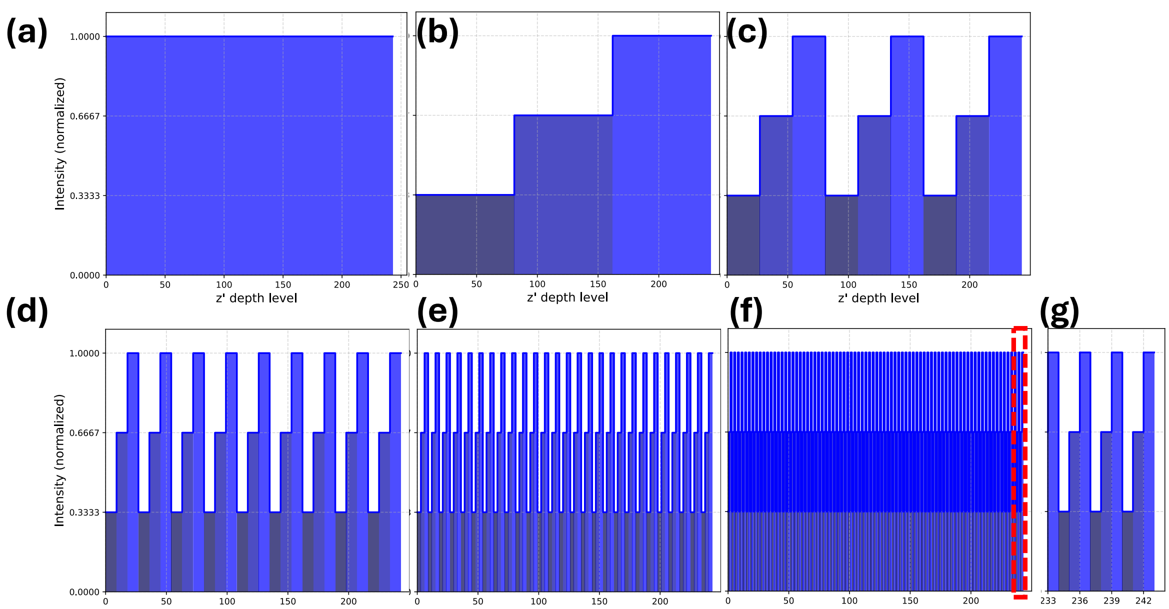

Supplementary Fig. 7 Illumination sequence used for producing the spatio-temporal structured illumination, the sequence goes from ***(a-f)*** *with each panel representing the intensity distribution in a single illuminated frame, each region of the illumination is refined at every frame until frame of panel* ***(f)*** *is repeated over a 5 frame period, i.e. a total of 10 frames of illumination cycle. Panel* ***(g)*** *shows the magnified region of the red region in* ***(f)****.*

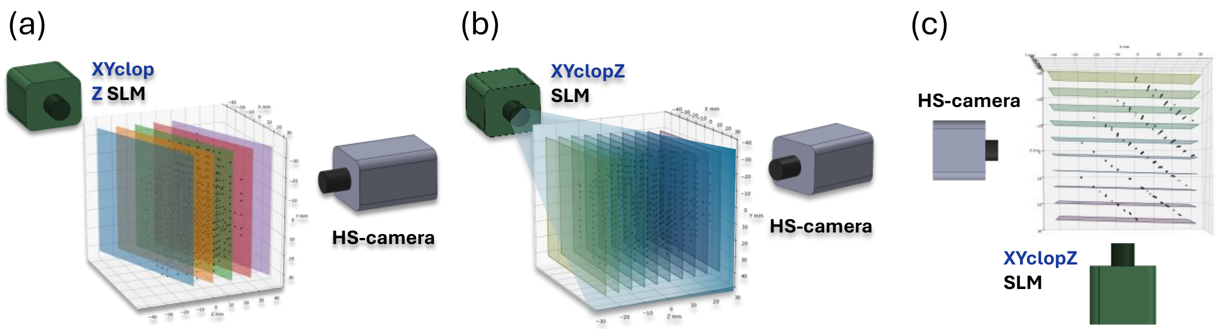

Supplementary Fig. 8 ***(a)*** *Reconstructed images of the calibration plate positioned at multiple discrete depth locations (color-coded by depth for clarity). Black crosses indicate the detected markers utilized for 3D coordinate system registration and spatial mapping.* ***(b)*** *3D perspective view and* ***(c)*** *top view of the reconstructed digital depth planes (z'). For visual clarity, only every 12th discrete digital depth level is displayed. The approximate positions of the camera and the XYclopZ-LPT spatial light modulator (SLM) are shown schematically relative to the reconstructed volume to aid reader orientation.*

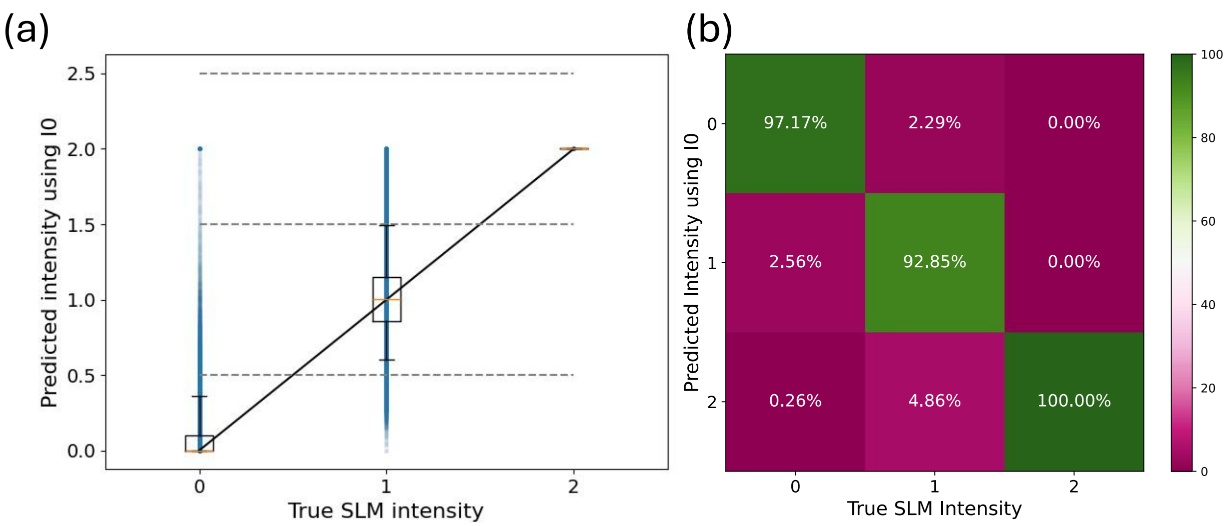

Supplementary Fig. 9 Intensity characterization for validation experiments using the von Kármán device. ***(a)*** *Typical Predicted Intensity response vs True structured illumination intensity for actual particle images, In this case, nearly 900,000 particles were used for this characterization over 200 frames.* ***(b)*** *Confusion matrix to present the portion of particles detected correctly with the light response polynomial curve.*

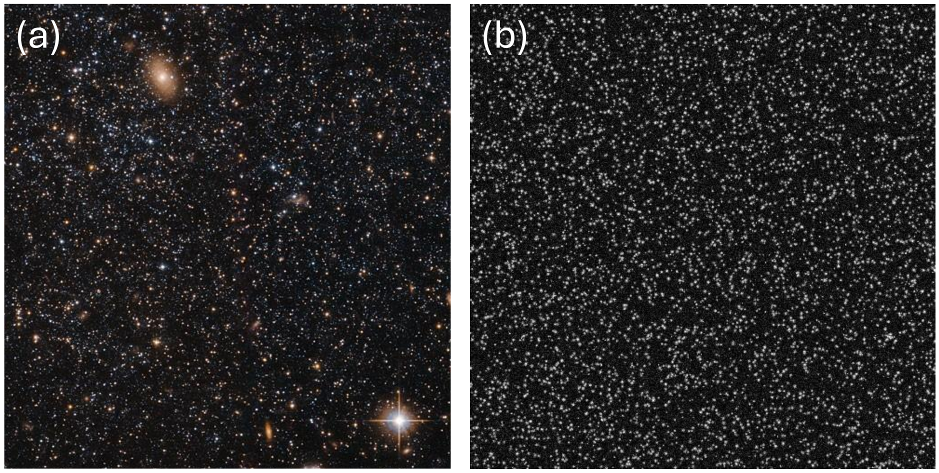

NASA Goddard, ESA/Hubble, Acknowledgment: Judy Schmidt. 2017

*Supplementary Fig. 10 Comparison between **(a)** a typical astronomical photometry image, and **(b)** a particle image velocimetry–particle tracking velocimetry (PIV–PTV) image. Panel **(a)** shows a representative deep-field or stellar-field image obtained with the NASA/ESA Hubble Space Telescope, retrieved from a publicly available archive [65]. Panel **(b)** illustrates a typical PIV–PTV recording used in the present study of the rigid-body rotation synthetic images at 0.025 ppp.*

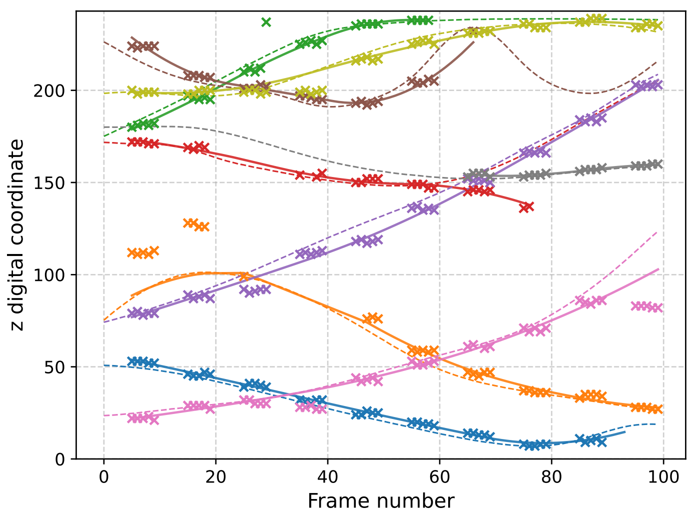

Supplementary Fig. 11 Estimated digital depth position ($\widehat{z'}$) versus time for nine randomly selected particle tracks in the synthetic Rayleigh–Bénard convection case at a seeding concentration of 0.01 particles per pixel (ppp). The cross markers (x) indicate the initial depth estimates prior to refinement. Solid lines show the final depth estimates ($\widehat{z'}$) obtained with the XYclopZ-LPT method after applying the RANSAC-based spline interpolation (described in section: Particle Intensity Characterization and Digital depth estimation (z')"). Dashed lines represent the ground-truth depth trajectories. Each particle track is consistently color-coded across initial estimates, refined estimates, and ground truth for direct comparison. Note initial spurious depth estimates have minimal impact on the final depth estimation.

Supplementary Videos

Supplementary V1. Sample clips of the synthetic particle images processed with XYclopZ-LPT. From left to right, Sink-like flow, Rigid-body rotation, Rayleigh-Benard convection.

Supplementary V2. Time evolution of particle tracks in the sink-like flow case, with 0.0125 ppp: Comparison between the ground truth (left) and the XYclopZ-LPT reconstruction (right). Tracks are colored by their out-of-plane velocity component w computed from the structured illumination.

Supplementary V3. Time evolution of particle tracks in the rigid-body rotation case, with 0.0125ppp: Comparison between the ground truth (left) and the XYclopZ-LPT reconstruction (right). Tracks are colored by their out-of-plane velocity component w computed from the structured illumination.

Supplementary V4. Time evolution of particle tracks in the Rayleigh-Benard convection with 0.01 ppp case: Comparison between the ground truth (left) and the XYclopZ-LPT reconstruction (right). Tracks are colored by their out-of-plane velocity component w computed from the structured illumination.

Supplementary V5. Raw sample frames collected from the Von Kármán device experiments. These frames were captured with camera 1 at 1000 fps, and are processed for both methods: STB and XYclopZ-LPT for a direct comparison. Please note that the image quality has been reduced to facilitate efficient online sharing.

Supplementary V6. Direct comparison between time-resolved 3D tracks reconstructed using a four-camera system with the DaVis "Shake-the-Box" algorithm (left) and a single-camera system with XYclopZ-LPT (right). Both methods demonstrate excellent agreement. Tracks are color-coded by their out-of-plane velocity component w (with respect to Camera 1).

Supplementary V7. Direct comparison of the recovered Eulerian velocity fields obtained from: (left) DaVis STB tracking followed by binning; (middle) XYclopZ-LPT tracking with RBF interpolation; and (right) XYclopZ-LPT tracking with PINN. The video shows the time evolution of isosurfaces of out-of-plane velocity component $w = +200\ mm/s$ (red) and $w = -200\ mm/s$ (blue).

Supplementary V8. Direct comparison of the recovered Eulerian vorticity field after differentiation of the Eulerian velocity field obtained from: (left) DaVis STB tracking followed by binning; (middle) XYclopZ-LPT tracking with RBF interpolation; and (right) XYclopZ-LPT tracking with PINN. The video shows the time evolution of iso-vorticity surfaces with magnitude $|\omega| = 45\frac{1}{s}$.

Supplementary V9. Representative raw image sequence from the live coral experiments, demonstrating the influence of ciliary activity near the tissue surface on the bulk flow and the generation of localized vortices.